JOURNAL OF MATERIALS SCIENCE 25 (1990) 3229–3235

Solid particle erosion of SiC–Al_2OC ceramics

S. GOCHNOUR, J. D. BRIGHT, D. K. SHETTY
Department of Materials Science and Engineering, University of Utah, Salt Lake City, Utah 84112, USA.

R. A. CUTLER
Ceramatec, Inc., 2425 South 900 West, Salt Lake City, Utah 84119, USA

Erosion rates of SiC–Al_2OC ceramics, with Al_2OC content varying from 5 to 75 wt%, were assessed using 240-grit alumina abrasive particles accelerated to a velocity estimated at 120 m sec^{-1} and impacting the target at normal incidence. The target ceramics varied in hardness from 27.1 GPa for SiC–5 wt% Al_2OC to 10.8 GPa for SiC–75 wt% Al_2OC, but the fracture toughness was essentially independent of composition ($K_{Ic} \sim 3.5$ MPa $m^{1/2}$). The erosion weight loss varied linearly with the test duration for all the ceramics and the erosion rate decreased systematically with increasing target hardness; the hardness dependence of the erosion rate was, however, much greater than the predictions of the currently available erosion models.

1. Introduction

Because of its high hardness and chemical inertness, SiC is increasingly used in applications that demand wear and corrosion resistance. In fluidized-bed combustors, for example, SiC tubes are being considered to replace high-temperature alloys to resist the severe conditions of erosion and corrosion at high temperatures [1]. As a result of this interest in wear applications, a number of studies have been directed to examine the performance of SiC in specific wear situations. Routbort and colleagues [2–5], Wiederhorn and Hockey [6] and Wada and Watanabe [7] studied solid particle erosion of SiC ceramics. Emphasis in the majority of these studies has been on evaluating the particle velocity and size dependence of the steady-state erosion rates and comparing them to the predictions of the elastic–plastic indentation fracture models of erosion [8,9]. The particle velocity and size exponents measured for reaction-bonded SiC were close to the theoretical expectations, while these exponents were anomalously low for hot-pressed SiC [2–6].

Evans *et al.* [8] and Wiederhorn and Hockey [6] examined the influence of hardness and fracture toughness of various target ceramics on their relative erosion rates in solid particle impact. In both of these studies, the dependence of the measured erosion rates on a combined fracture toughness and hardness parameter was greater than the theoretical expectations based on the indentation fracture models. The effects of target hardness and fracture toughness were, however, not separated. More recently, Wada and Watanabe [7] conducted erosion tests on SiC with different impacting particles of varying hardness. The erosion rate of the same target SiC increased very significantly with an increase in the hardness of the impacting particles relative to the hardness of the target SiC.

Jackson *et al.* [10] have sintered SiC at temperatures between 1850 and 1950° C using a transient liquid phase produced by the carbothermal reduction of Al_2O_3 by Al_4C_3. The resulting ceramic was fine grained (average grain size less than 5 μm) and consisted of SiC (starting polymorphs) and Al_2OC as the two major phases and minor amounts of Al_2O_3 and WC. The properties of the hot-pressed ceramics varied with the amount of Al_2OC, but at an optimum composition of about 5 to 10 wt% Al_2OC, the strength (σ_f = 660 MPa), hardness (H = 27.1 GPa) and fracture toughness (K_{Ic} = 3.1 MPa $m^{1/2}$) obtained were comparable or superior to the corresponding properties of commercial grades of sintered SiC [10].

The present paper summarizes the results of an investigation of the erosion behaviour of the above SiC–Al_2OC ceramics under solid particle impact. The primary objective of this study was to examine the influence of a systematic variation of the microstructures and properties of a class of ceramics within the same generic family on their erosion response. A second objective was to compare the erosion response of SiC–Al_2OC ceramics of optimum composition with the response of several commercial sintered and hot-pressed grades of SiC.

2. Materials and test procedures

2.1. SiC–Al_2OC ceramics

The processing of the SiC–Al_2OC ceramics via liquid-phase sintering has been described by Jackson *et al.* [10]. Ceramics with Al_2OC content varying from 5 to 75 wt % were fabricated and characterized with respect to a number of properties. Some of these properties relevant to erosion are listed in Table I. Fracture toughness of the ceramics was relatively invariant with composition, but all the other properties such as density, hardness, bend strength, elastic modulus and coefficient of thermal expansion, varied systematically with the Al_2OC content.

Figs 1a to c show the microstructures of the cer-

0022–2461/90 $03.00 + .12 © *1990 Chapman and Hall Ltd.*

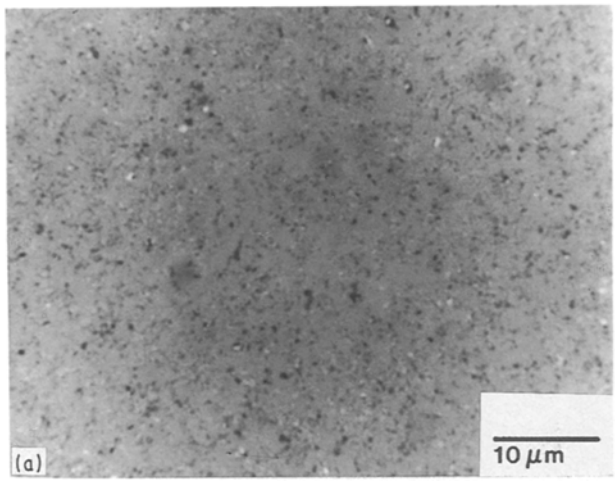

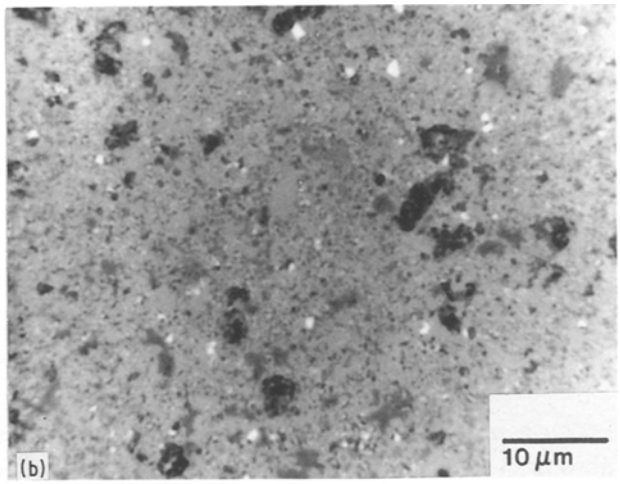

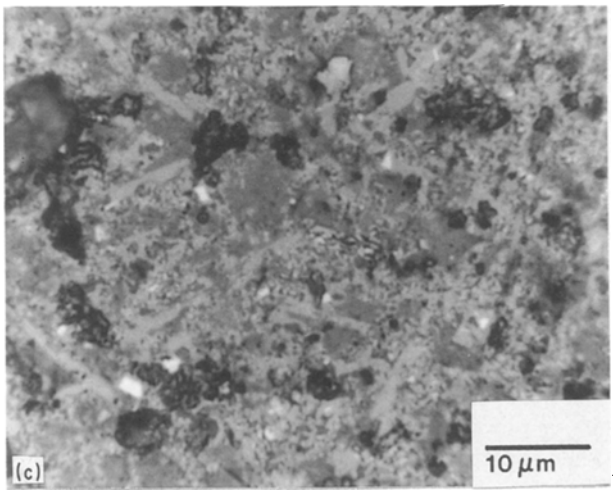

Figure 1 Microstructures of selected SiC–Al_2OC ceramics: (a) SiC–5 wt % Al_2OC, (b) SiC–30 wt % Al_2OC, and (c) SiC–75 wt % Al_2OC.

amics with 5, 30 and 75 wt % Al_2OC, respectively. There are two major phases in the microstructure. The light grey coloured phase is SiC. It is the predominant phase in the 5 and 30 wt % Al_2OC ceramics and appears as a minor phase in the form of elongated grains in the SiC–75 wt % Al_2OC ceramic (see Fig. 1c). The dark grey coloured phase is Al_2OC. Because of its low hardness relative to that of SiC, it is readily pulled out during grinding and polishing. This grain pull-out appears as dark pores in the microstructures of Figs 1b and c. In addition to these major phases, there are some minor phases apparent in the microstructures. The bright coloured particles in the microstructure are WC picked up from the milling media.

2.2. Erosion tests

The erosion test apparatus, test conditions (except particle velocity) and the test procedure used in this study were close to the specifications of ASTM standard G76-83 [11]. Fig. 2 is a schematic illustration of the test apparatus. The major components of the apparatus included a steel hopper that stored the abrasive particles, a motor-driven screw feeder that transported the abrasives at a uniform rate and a cylindrical chamber with a conical section attached to a nozzle in which the abrasive particles were accelerated to a steady-state velocity using air flow. The feed rate of the abrasive particles was controlled by controlling the speed of the motor used to turn the screw feeder. The abrasive flux was uniform during the tests and was controlled at 2.25 g min^{-1}. The nozzle used in the erosion apparatus was a cemented WC–Co cylinder (Grade K-701, Kennametal Inc, Latrobe, Pennsylvania), 50 mm long with a 1 mm axial hole along its length. The acceleration of the abrasive particles and the final steady-state velocity were controlled by adjusting the pressure of the incoming air drawn from a cylinder. All the tests in this study were conducted at a fixed pressure of 0.48 MPa (70 p.s.i.). The entire apparatus, including the hopper, was under the set pressure during erosion tests. The velocity of the abrasive particles attained at this pressure was not directly measured. It was, however, estimated as 120 m sec^{-1}. This was based on steady state erosion rates for 1020 steel, a standard reference target for which erosion rate data are reported in the ASTM standard [11] for measured velocities of 30 and 70 m sec^{-1}. A power-law relationship between steady-state erosion rate and particle velocity was assumed for estimating the velocity by extrapolation.

The abrasive particles used in the erosion tests were 240-grit alumina (type 54 Alundum, Norton Company, Worcester, Massachusetts). Fig. 3 shows a scanning electron micrograph of the alumina abrasive particles. The particles are angular with sharp edges and corners. Typical size distribution was as follows: 100% between 20 and 83 μm, 50% between 42 and 57 μm, 50 % coarser than 48 μm. Fresh alumina abrasive particles were used in each test and were not recycled.

TABLE I Properties of the SiC–Al_2OC ceramics used in the erosion experiments

Ceramic (wt % Al_2OC)	Density (g cm^{-3})	Hardness (GPa)	Fracture toughness (MPA $m^{1/2}$)	Young's modulus (GPa)
5	3.29	27.1 ± 0.64	3.03 ± 0.15	
10	3.25	23.2 ± 1.08	3.08 ± 0.31	353
15	3.26	20.2 ± 0.54	3.50 ± 0.32	321
20	3.30	20.8 ± 0.45	3.48 ± 0.19	356
30	3.23	17.1 ± 0.16	3.84 ± 0.40	303
40	3.19	16.6 ± 1.40	3.45 ± 0.48	308
50	3.18	13.7 ± 0.34	3.36 ± 0.30	255
75	3.08	10.8 ± 0.35	3.67 ± 0.45	194

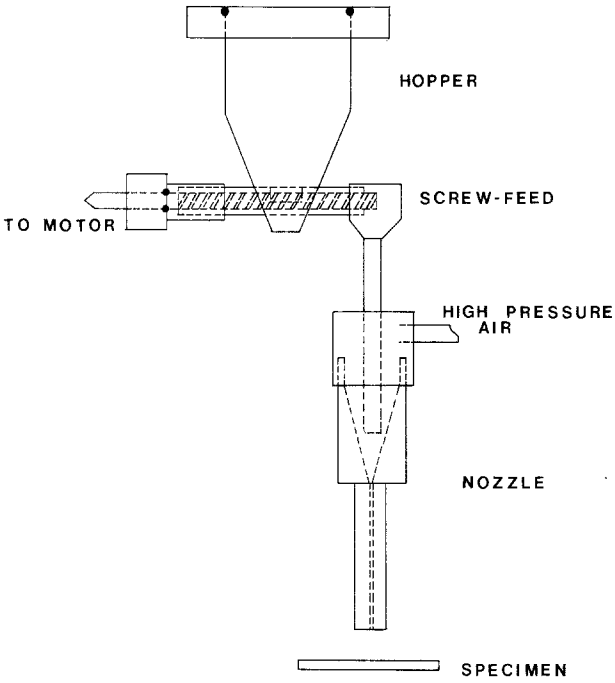

Figure 2 Schematic drawing of the erosion test apparatus.

The erosion test specimens of SiC–Al_2OC ceramics were in the form of rectangular bars, 3 mm by 4 mm by 45 mm. The specimen surfaces to be eroded were ground flat using a metal-bonded 30 μm diamond wheel followed by a metal-bonded 15 μm diamond wheel. The ground surfaces of the specimens were successively polished using 9, 6 and 1 μm diamond paste.

In a typical erosion test, the abrasive feed rate and the air inlet pressure were adjusted to the desired values and when steady-state conditions were attained, the test specimen surface was exposed to the high-velocity jet. The target surface was located at 10 $\pm$ 1 mm from the nozzle end. The test periods ranged from a few seconds to several minutes, depending upon the erosion rates of the target materials, to obtain weight losses ranging from 0.5 to 5 mg. All test specimens were cleaned in acetone in an ultrasonic bath for 5 min to remove any loose target material or abrasive particles that adhered to the surface. Specimens were weighed using a microbalance (Model AE240, Analytical Balance, Mettler Instrument Corp., Hightstown, New Jersey) with a load sensitivity of 10 μg.

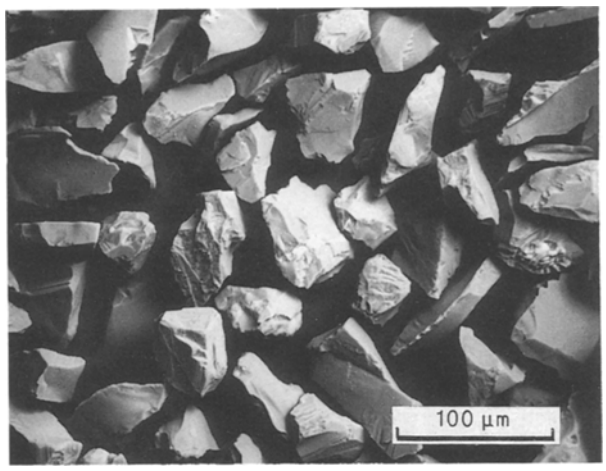

Figure 3 240-grit alumina abrasive used in the erosion tests.

3. Erosion test results

3.1. Erosion craters

Figs 4a and b show two typical craters produced on test surfaces of SiC–5 wt % Al_2OC and SiC–50 wt % Al_2OC, respectively, in erosion tests of 5 min duration. The crater periphery was circular with a diameter of about 2.5 mm. Within the crater, the wear profile was not always axially symmetric. One example is the facetted crater shown in Fig. 4b for SiC–50 wt % Al_2OC. Such asymmetric craters were, however, exceptions rather than the rule.

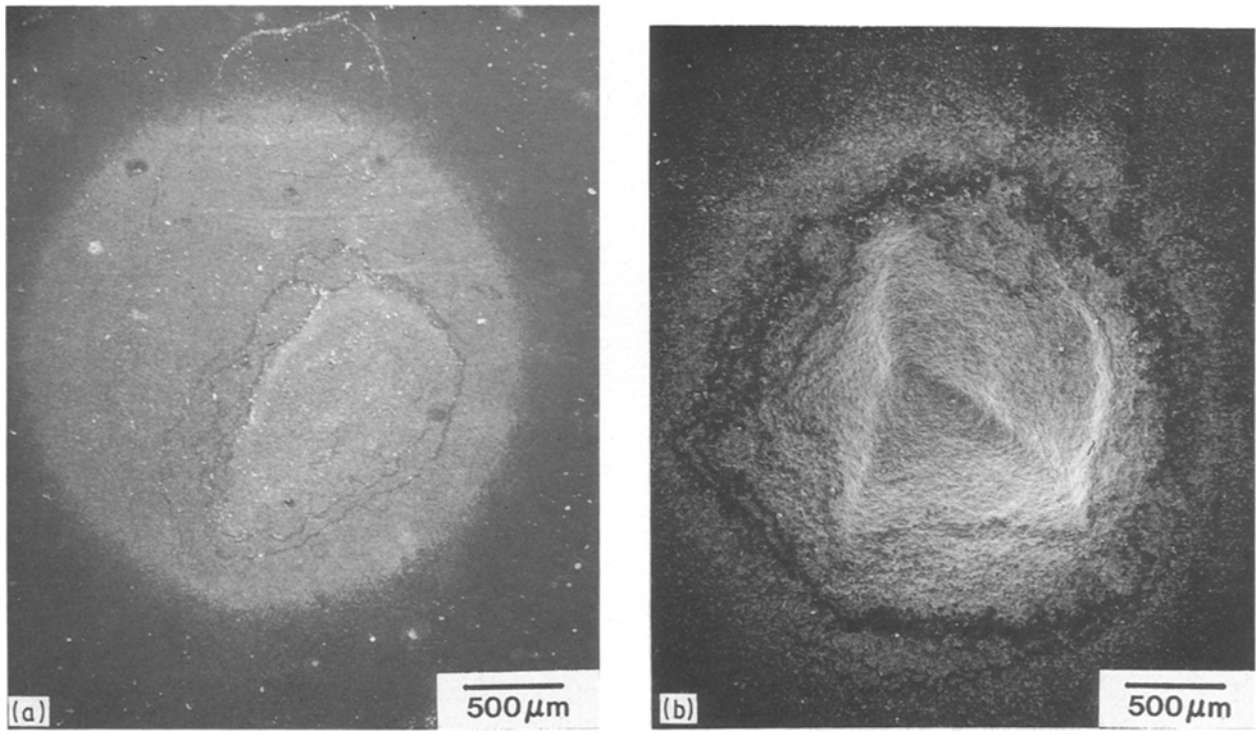

Figure 4 Typical erosion craters in SiC–Al_2OC ceramics: (a) SiC–5 wt % Al_2OC and (b) SiC–50 wt % Al_2OC.

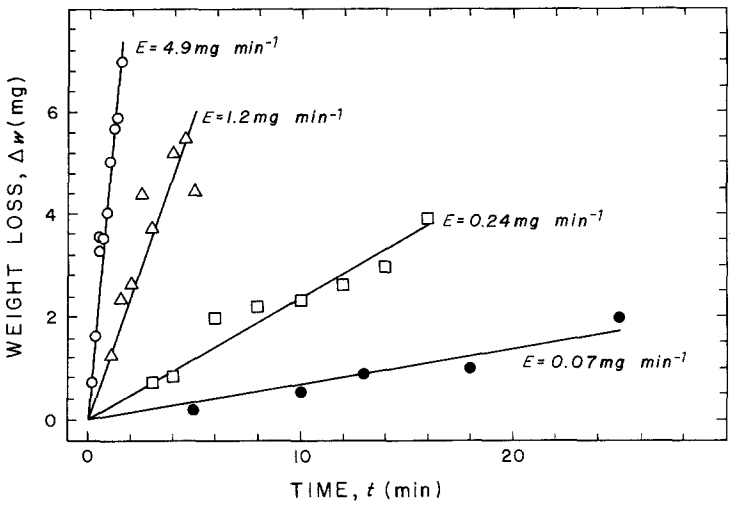

Figure 5 Linear variation of total weight loss as a function of time in solid particle erosion of SiC–Al_2OC ceramics. Al_2OC content (wt %): (●) 5, (□) 30, (△) 50, (○) 75.

3.2. Weight loss measurements

Weight loss of the targets as a function of test duration are plotted in Fig. 5 for SiC–Al_2OC ceramics containing 5, 30, 50 and 75 wt % Al_2OC. The weight loss varied linearly with time for all the target ceramics. Erosion rates (E), defined as weight loss per unit time, (mg min^{-1}) were evaluated by linear regression based on least squares deviation for straight lines passing through the origin. The erosion rates ranged from 0.07 to 4.9 mg min^{-1} for SiC ceramics with Al_2OC content ranging from 5 to 75 wt %.

3.3. Composition dependence of erosion rates

Fig. 6 shows a semilogarithmic plot of the erosion rate as a function of weight per cent of Al_2OC. The erosion rate generally increased with increasing Al_2OC content with one exception; SiC–Al_2OC ceramics with Al_2OC contents of 15, 20 and 30 wt % had nearly the same erosion rates.

3.4. Dependence of erosion rates on hardness

Because hardness and fracture toughness are the material properties that influence erosion the most, and because fracture toughness did not vary significantly with the composition of the SiC–Al_2OC ceramics, the erosion rates were correlated only with hardness. Fig. 7 shows a plot of the volume of the target eroded per particle impact, v_t, normalized by the particle volume, v_p, against the target hardness, H_t, normalized with respect to the hardness of the alumina abrasive particles, H_p = 20 GPa. In this plot, eroded volume per particle impact is plotted because theoretical models of erosion are often expressed in terms of eroded volume rather than eroded weight [8, 9]. A normalized plot such as Fig. 7 is also convenient for comparing the present results with similar results in the literature. Values of v_t were calculated from the erosion rates, E, using the densities of the target ceramics and of the alumina abrasives (3.95 g cm^{-3}), the steady-state flux of the alumina abrasives (2.25 g min^{-1}), and by assuming spherical shape and uniform median size for the abrasive particles (48 μm).

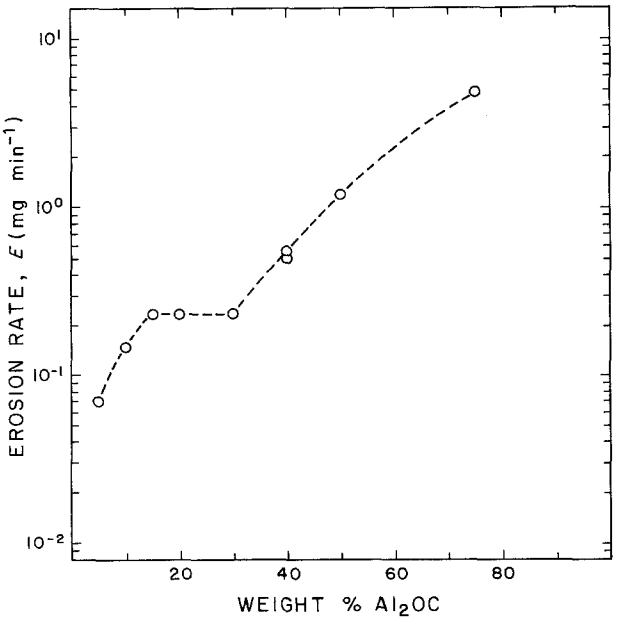

Figure 6 Variation of erosion rate as a function of Al_2OC content of SIC–Al_2OC ceramics.

The inverse linear correlation on the log–log plot of Fig. 7 suggests the following power-law relationship

$$\frac{v_t}{v_p} = A\left[\frac{H_p}{H_t}\right]^n \quad (1)$$

where A is an experimental constant that corresponds to the normalized eroded volume when $H_p = H_t$. A hardness exponent, n = 4.4 and $A = 1.283 \times 10^{-4}$, were evaluated by fitting the power law over the entire range of hardness and erosion rates and this fit is shown by the solid straight line in Fig. 7. This procedure ignored the plateau in erosion rates at intermediate hardness levels which might possibly correspond to a transition regime. The hardness exponents in the high and low hardness regimes ($\sim$5 and 5.3, respectively) were, however, not significantly different from the average value measured over the entire range.

The dependence of the erosion rate on the relative hardness observed in this study can be compared with two similar studies on other ceramic systems. Wada and Watanabe [7] measured erosion rates of SiC, Si_3N_4, ZrO_2 and glass with different erodent particles of varying hardness. Their erosion data on SiC obtained with erodent particles of different hardness are also shown in Fig. 7. The normalized eroded volumes of SiC measured in their study are higher than

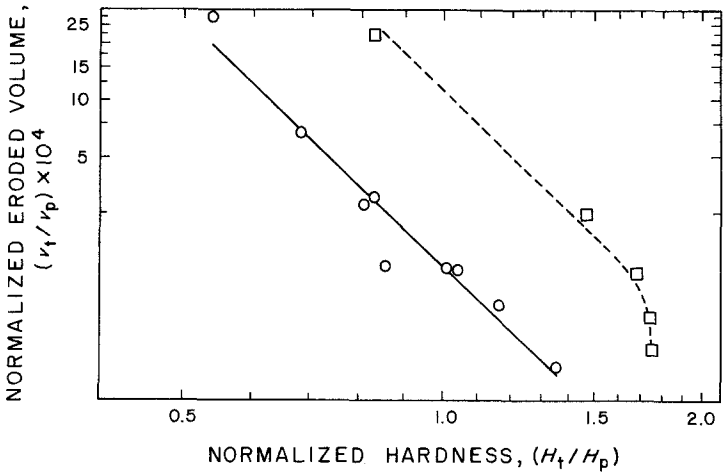

Figure 7 Dependence of the erosion volume loss per particle impact on the hardness of (○) SiC–Al_2OC ceramics, compared to (□) SiC [7].

the present results at the same value of the relative hardness. This is likely due to the higher particle velocity (300 m sec^{-1}) as well as the larger erodent particle size (~325 to 385 μm) used in their experiments. In the relative hardness range that is common to both the studies, the hardness exponents are comparable. However, the results of Wada and Watanabe show a much greater decrease in the normalized eroded volume for relative hardness values greater than about 1.5. Their data on Si_3N_4 and ZrO_2 also showed similar rapid decrease in erosion rates, but this occurred at $H_t/H_p = 1$. Shetty *et al.* [12] have also observed a rapid decrease in erosion rate at $H_t \simeq H_p$ in slurry erosion of ceramics using fused silica abrasive.

Landingham and Taylor [13] measured erosion rates of several ceramics with different erodent particles. The hardness of the target ceramics relative to the hardness of the erodent particles was varied in the range 0.5 to 3. The normalized erosion rate (i.e. weight loss of the target per unit weight of the erodent particles) showed an excellent inverse power-law correlation with the hardness of the target normalized by the particle hardness. The hardness exponent was, however, only about 2.

High hardness exponents are common in the erosion response of cermets. In slurry erosion, Shetty *et al.* [12] measured a hardness exponent of 8.3 for WC–Co alloys with a uniform WC grain size of about 1 μm and hardness ranging from 9.75 to 16.72 GPa (corresponding to cobalt volume fraction varying from 0.369 to 0.051). Erosion test results of Uuemyis *et al.* [14] and Conrad *et al.* [15] on WC–Co alloys also showed similar strong dependence of erosion rates on hardness or cobalt volume fraction.

3.5. Comparison of erosion rates of different SiC ceramics

Fig. 8 compares the erosion weight loss as a function of time for three SiC ceramics, two of which are commercially available. The three ceramics were sintered by three different mechanisms as identified in the figure and their microstructures also differed slightly with respect to the nature and type of second-phase distributions at the grain boundaries. The sintered SiC was essentially single phase and was densified by pressureless sintering using additives which are believed to promote solid state sintering. The liquid-phase sintered SiC was densified using an additive mixture of Al_2O_3 and Y_2O_3, which formed a liquid at the sintering temperature. The hot-pressed SiC had Al_2O_3 as the additive. The sintered and the hot-pressed SiCs are commercially available, while the liquid-phase sintered SiC is an experimental grade currently in development [16]. The relative erosion rates varied by nearly an order of magnitude among the three grades with the sintered grade showing the highest erosion rate. The experimental liquid-phase pressureless sintered SiC showed a surprisingly low erosion rate despite the presence of a grain-boundary phase derived from the liquid used to assist sintering. Comparison of Figs 5 and 8 reveals that the erosion rate of hot-pressed SiC–5 wt % Al_2OC is comparable to that of the most erosion resistant SiC currently available from commercial sources.

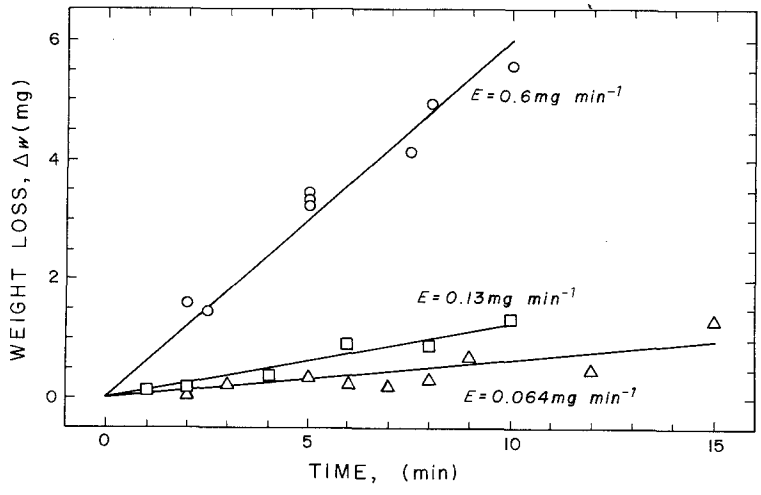

Figure 8 Comparison of the erosion weight losses of three SiC ceramics obtained from three different sources. (○) SiC (sintered), (□) SiC (hot-pressed), (△) SiC (liquid-phase sintered).

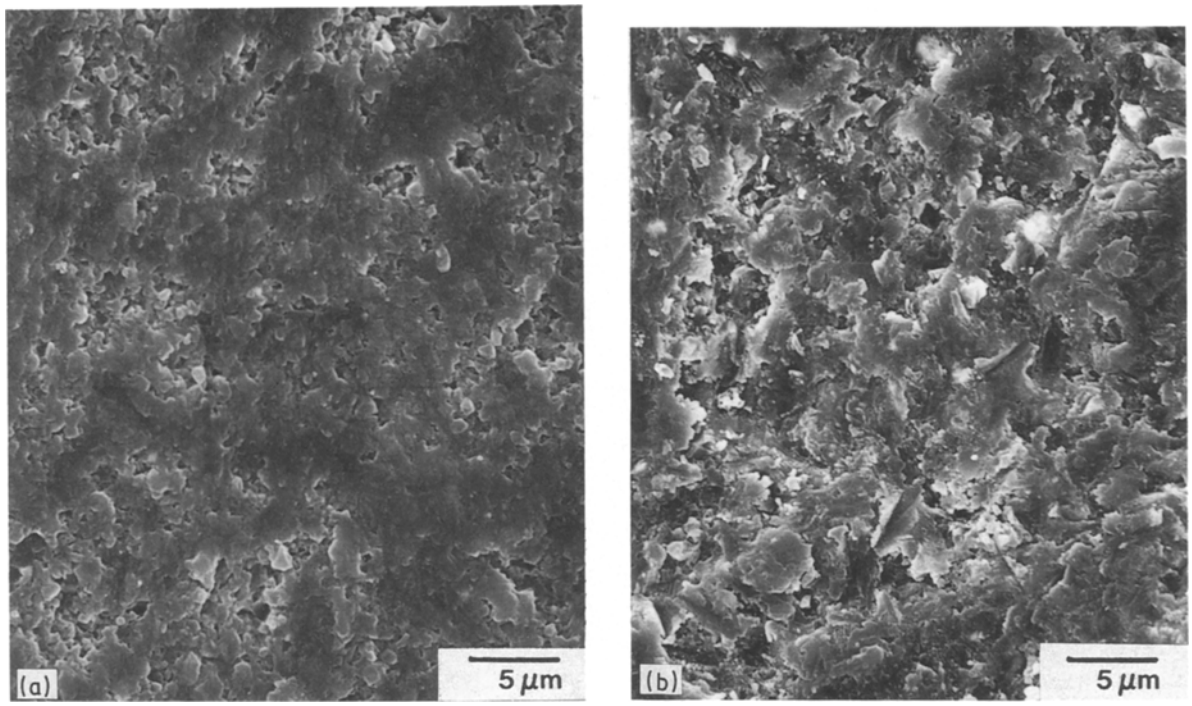

Figure 9 Eroded surfaces on SiC–Al_2OC ceramics: (a) SiC–5 wt % Al_2OC, (b) SiC–50 wt % Al_2OC.

4. Discussion

The mechanism of solid particle erosion in brittle ceramics that has received the most attention is microfracture via elastic–plastic indentation and formation of subsurface lateral cracks below the plastic zone. Two analytical formulations for the volume of the target eroded per particle impact have been advanced. Wiederhorn and Lawn [17] and Ruff and Wiederhorn [9] treated particle impact as a quasi-static event in which the kinetic energy of the particle is assumed to be absorbed completely by plastic flow when a particle impacts the surface. Further, by assuming that the lateral crack size is proportional to the radial crack size, and that the depth of the lateral cracks is proportional to the maximum particle penetration, the following expression for the volume of the target eroded per particle impact was derived

$$v_t \propto v^{22/9} r^{11/3} \rho^{11/9} K_c^{-4/3} H_t^{1/9} \quad (2)$$

where v is the particle velocity, r the particle radius, ρ the particle density, and K_c the fracture toughness of the ceramic target.

Evans *et al.* [8], on the other hand, included a correction for dynamic stress wave effects in the calculation of the particle impact force. Their final expression for the eroded volume per particle impact was

$$v_t \propto v^{19/6} r^{11/3} \rho^{19/12} K_c^{-4/3} H_t^{-1/4} \quad (3)$$

It is obvious from Equations 2 and 3 and the erosion results of this study that the indentation microfracture models are inconsistent with the large hardness exponent obtained for SiC–Al_2OC ceramics. This was also confirmed by scanning electron microscope examination of the eroded surfaces. Figs 9a and b show the eroded surfaces of SiC–5 wt % Al_2OC and SiC–50 wt % Al_2OC, respectively. The eroded surface on SiC–5 wt % Al_2OC showed smooth zones with almost a polished appearance intermingled with regions of grain pull-out. The smooth zones are very likely the harder SiC phase, while the grain pull-out regions correspond to softer Al_2OC phase. The eroded surface on SiC–50 wt % Al_2OC showed severe damage with only isolated regions of smooth zones. As seen in Fig. 9b, there was evidence for localized cutting/gouging and formation of severely deformed platelets or flakes. But there was no evidence of brittle microfracture as envisaged in the indentation fracture models of erosion. It is likely that the erodent particle size and velocity, and, therefore, the kinetic energy of the impacting particles, employed in the erosion experiments was below the critical value required to initiate lateral cracks, at least on a large scale. In support of this idea, it is noted that lateral cracking has been generally observed on eroded surfaces of ceramics when the erodent particles are larger than about 100 μm. Indentation fracture theories do postulate a threshold kinetic energy of particle impact that is necessary to initiate erosion in the form of lateral cracking [9].

Below the microfracture threshold, erosion of ceramics is generally believed to occur by such plastic deformation mechanisms as plastic cutting, extrusion and platelet formation. Many of these mechanisms were initially proposed for metals. Several quantitative models have been formulated to express the volume loss of the target in terms of the particle size, velocity and angle of impact and the properties of the target. Ruff and Wiederhorn [9] have reviewed these mechanisms applicable to both metals and ceramics. Dynamic hardness of the target is one of the material properties that influence erosion rate. However, these models typically predict a hardness exponent (n in Equation 1) of 1 or 1.5. Thus, the large hardness exponent observed in the present study is not consistent with the plastic deformation models either.

The majority of the theoretical models of erosion, proposed for ceramics or metals, have been explicitly

developed for homogeneous, single-phase materials. SiC–Al_2OC ceramics clearly do not fit this category. Their microstructures are complex, and, in particular, they consist of two major phases with widely differing properties such as hardness and modulus. In this sense, they are similar to glass-bonded ceramics or metal-bonded cermets. The Al_2OC phase, with its low hardness, acts as a "binder" for the much harder SiC phase during liquid-phase sintering. In such microstructures, the erosion rate of the composite is not a simple weighted average of the intrinsic erosion rates of the individual phases. At large volume fraction of the hard phase, the Al_2OC phase is shielded from the impacting particles by the surrounding hard phase. On the other hand, at small volume fractions, the hard phase provides disproportionately low protection from erosion due to undercutting and loss of whole grains. These microstructural effects lead to a highly nonlinear variation of erosion rate with the relative amounts of the two phases and, therefore, the bulk hardness of the composite ceramic. This is believed to be the origin of the unusually strong dependence of the erosion rate on the bulk hardness of the SiC–Al_2OC ceramics. Shetty *et al.* [18] used this concept to analyse quantitatively the dependence of slurry erosion rate of WC–Co cermets on the volume fraction of cobalt.

From a comparison of the erosion rates of different grades of SiC (Fig. 8) it is evident that liquid-phase sintered SiC ceramics compare very favourably in erosion performance with conventional pressureless sintered or hot-pressed SiCs. In this connection, it is interesting to note that sintered SiC, which is essentially a single-phase ceramic without any grain-boundary phase, exhibited an erosion rate that was about an order of magnitude greater than the erosion rates of the other three silicon carbide ceramics that contained second phases (i.e. hot-pressed SiC containing Al_2O_3, liquid-phase pressureless sintered SiC which contained Al_2O_3 and Y_2O_3 and hot-pressed SiC–5 wt % Al_2OC). The high erosion rate of sintered SiC was also consistent with the appearance of its eroded surface. There was evidence of microfracture on the eroded surface. It is suggested that the particle impact conditions used in the erosion experiments corresponded to the microfracture regime for the sintered SiC. In other words, this ceramic has a lower microfracture threshold as compared to the other three ceramics. This is consistent with its low fracture toughness ($K_c \sim 2.8\,MPa\,m^{1/2}$) in relation to the fracture toughness of the commercially available hot-pressed SiC and the experimental liquid-phase pressureless sintered SiC ($K_c \sim 4\,MPa\,m^{1/2}$).

5. Conclusions

1. SiC–Al_2OC ceramics exhibit erosion rates that vary significantly with composition and bulk hardness of the ceramics.

2. The hardness dependence of the erosion rates of SiC–Al_2OC ceramics is not consistent with the predictions of the available erosion models.

3. The two-phase nature of the microstructure and the large differences in the intrinsic properties of the two phases lead to a highly non-linear variation of the erosion rate with composition and account for the large hardness exponent.

4. Erosion resistance of liquid-phase sintered ceramics are comparable to that of the most erosion-resistant SiC ceramic available from commercial sources.

Acknowledgements

The research reported in this paper was partially supported by the Research Committee of the University of Utah and by the US Department of Energy under contract no. DE-FG02-87ER45312 at the University of Utah.

References

1. H. W. CARPENTER, *Am. Ceram. Soc. Bull.* **63** [8] 1015, Abstract only.
2. J. L. ROUTBORT and R. O. SCATTERGOOD, *J. Amer. Ceram. Soc.* **63** (1980) 593.
3. J. L. ROUTBORT, R. O. SCATTERGOOD and A. P. L. TURNER, *Wear* **50** (1980) 363.
4. J. L. ROUTBORT and A. P. L. TURNER, *ibid.* **84** (1983) 381.
5. J. L. ROUTBORT and H. J. MATZKE, *J. Mater. Sci.* **18** (1983) 1491.
6. S. M. WIEDERHORN and B. J. HOCKEY, *ibid.* **18** (1983) 766.
7. S. WADA and N. WATANABE, *Yogyo-Kyokai-Shi* **95** (1987) 573.
8. A. G. EVANS, M. E. GULDEN and M. ROSENBLATT, *Proc. R. Soc. Lond. A* **361** (1978) 343.
9. A. W. RUFF and S. M. WIEDERHORN, "Erosion By Solid Particle Impact", in "Treatise on Materials Science and Engineering", Vol. 16, "Erosion", edited by C. M. Preece (Academic Press, New York, 1979) pp. 69-126.
10. T. B. JACKSON, A. C. HURFORD, S. L. BRUNER and R. A. CUTLER, "SiC-Based Ceramics with Improved Strength", in "Silicon Carbide", edited by J. W. Cawley and C. Semler (The American Ceramic Society, Columbus, Ohio, 1989) pp. 227-40.
11. ASTM Standard G76-83, "Standard Practice for Conducting Erosion Tests by Solid Particle Impingement Using Gas Jets", in "Annual Book of ASTM Standards", Section 3, Vol. 03.02 (American Society for Testing and Materials, Philadelphia, Pennsylvania, 1986) pp. 443-50.
12. D. K. SHETTY, I. G. WRIGHT and J. T. STROPKI, *Trans, ASLE* **28** (1985) 123.
13. R. L. LANDINGHAM and R. W. TAYLOR, "Materials Development and Evaluation for the Ceramic Helical Expander" in "Energy and Ceramics", edited by P. Vincenzini (Elsevier Scientific 1980) pp. 494-512.
14. K. H. UUEMYIS, I. KLEIS, V. TUMANOV and T. TILDEMANN, *Poroshkovaya Metallurgia* **135** (1974) 98.
15. H. CONRAD, D. McCABE G. A. SARGENT, "Effects of Microstructure on the Erosion of WC–Co Alloys", Proceedings of the International Conference on the Science of Hard Materials edited by R. K. Viswanadham, D. J. Rowcliffe and J. Gurland (Plenum Press, New York, 1983) pp. 775–96.
16. R. A. CUTLER and T. B. JACKSON, "Liquid Phase Sintered Silicon Carbide", in Proceedings 3rd International Symposium on Ceramic Materials and Components for Engines, Las Vegas, edited by V. J. Tennery *Am. Ceram. Soc.* (1989) pp. 304–18.
17. S. M. WIEDERHORN and B. R. LAWN, *J. Amer. Ceram. Soc.* **62** (1979) 66.
18. D. K. SHETTY, I. G. WRIGHT and A. H. CLAUER, *Wear* **114** (1987) 1.

Received 14 March
and accepted 30 August 1989